Geophys. J. Int. (1993) **113,** 260–267

RESEARCH NOTE

The source parameters of the Çubukdağ (W. Turkey) earthquake of 1986 October 11

Tuncay Taymaz

Department of Geophysics, Mining Faculty, Istanbul Technical University, Maslak 80626, *Istanbul, Turkey*

Accepted 1992 August 19. Received 1992 February 10; in original form 1991 July 19

SUMMARY

Long period *P* and *SH* waveforms and first motion polarities of *P* waves were used to determine the source parameters of the Çubukdağ (in the eastern section of the Büyük Menderes graben) earthquake of 1986 October 11. The waveforms used in this event include the WWSSN, and the digitally recorded seismograms of the DWWSSN, SRO and ASRO networks. The minimum misfit solution obtained by the inversion of teleseismic body waveforms are better constrained that those of the previously published Harvard Centroid–Moment Tensor solution, and are in good agreement with field observations and the local geometry of the graben.

Key words: Büyük Menderes graben, Çubukdağ, faulting, waveform inversion, W. Turkey.

1 INTRODUCTION

The Aegean Sea, and the surrounding coastal areas of western Turkey and Greece, is one of the most seismically active and rapidly deforming continental regions (Fig. 1a). Its present day activity is manifest in its high seismicity and by the dramatic influence of large active normal faults on the topography, geomorphology and movement of the coastline relative to sea level. As the North Anatolian Fault (NAF) system enters the northeastern Aegean region it splits into several subparallel branches that cross NW Turkey and the north Aegean Sea, each of which develops a normal component of slip as well as the predominant right-lateral slip (McKenzie 1978; Barka & Kadinsky-Cade 1988; Taymaz, Jackson & McKenzie 1991a). The westward motion of Turkey relative to Eurasia is in turn related to the collision between Arabia and Eurasia in the Caucasus and eastern Turkey, which began about 12 Ma in the mid-Miocene (Dewey *et al.* 1986; Philip *et al.* 1989). NW Turkey and the Sea of Marmara are dominated by nomral faulting with an E–W strike, and right-lateral strike–slip faulting with an ENE strike. Within the Aegean extensional province, many normal faults are also known to be active, from geomorphological, seismological, and marine geophysical observations (McKenzie 1978; Lalechos & Savoyat 1979; Brooks & Ferentinos 1980; Lybéris 1984). Likely N–S extension rates across the Aegean as a whole are in the range 40–60 mm yr^{-1}, much of which might occur in the north and central Aegean where the seismicity is most intense (Fig. 1a). The main active normal faults in western Turkey strike east–west, have a spacing of up to 100 km. The Çubukdağ earthquake occurred in the vicinity of the Büyük Menderes graben (Fig. 1b–d).

2 DATA REDUCTION

I used both *P* and *SH* waveforms and first-motion polarities of *P* waves to constrain earthquake source parameters. The waveforms used in this earthquake include the WWSSN, and the digitally recorded seismograms of the DWWSSN, SRO and ASRO networks. The approach I followed is that described by Molnar & Lyon-Cáen (1989), and was also used in studies of earthquakes in the Hellenic Trench and the Aegean by Taymaz, Jackson & Westaway (1990) and Taymaz *et al.* (1991a). I compared the shapes and amplitudes of long period *P* and *SH* waveforms recorded by WWSSN stations in the distance range 30°–90° with synthetic waveforms. To determine source parameters I used McCaffrey & Abers's (1988) version of Nábělek's (1984) inversion procedure, which minimizes in a weighted least-squares sense the misfit between observed and synthetic seismograms (McCaffrey & Nábělek 1987; Nelson, McCaffrey & Molnar 1987; Fredrich, McCaffrey & Denham 1988). Seismograms are generated by combining direct (*P* or *S*) and reflected (*pP* and *sP*, or *sS*) phases from a point source embedded in a given velocity structure. Receiver structures are assumed to be homogeneous half spaces. Amplitudes are adjusted for geometrical spreading, and for

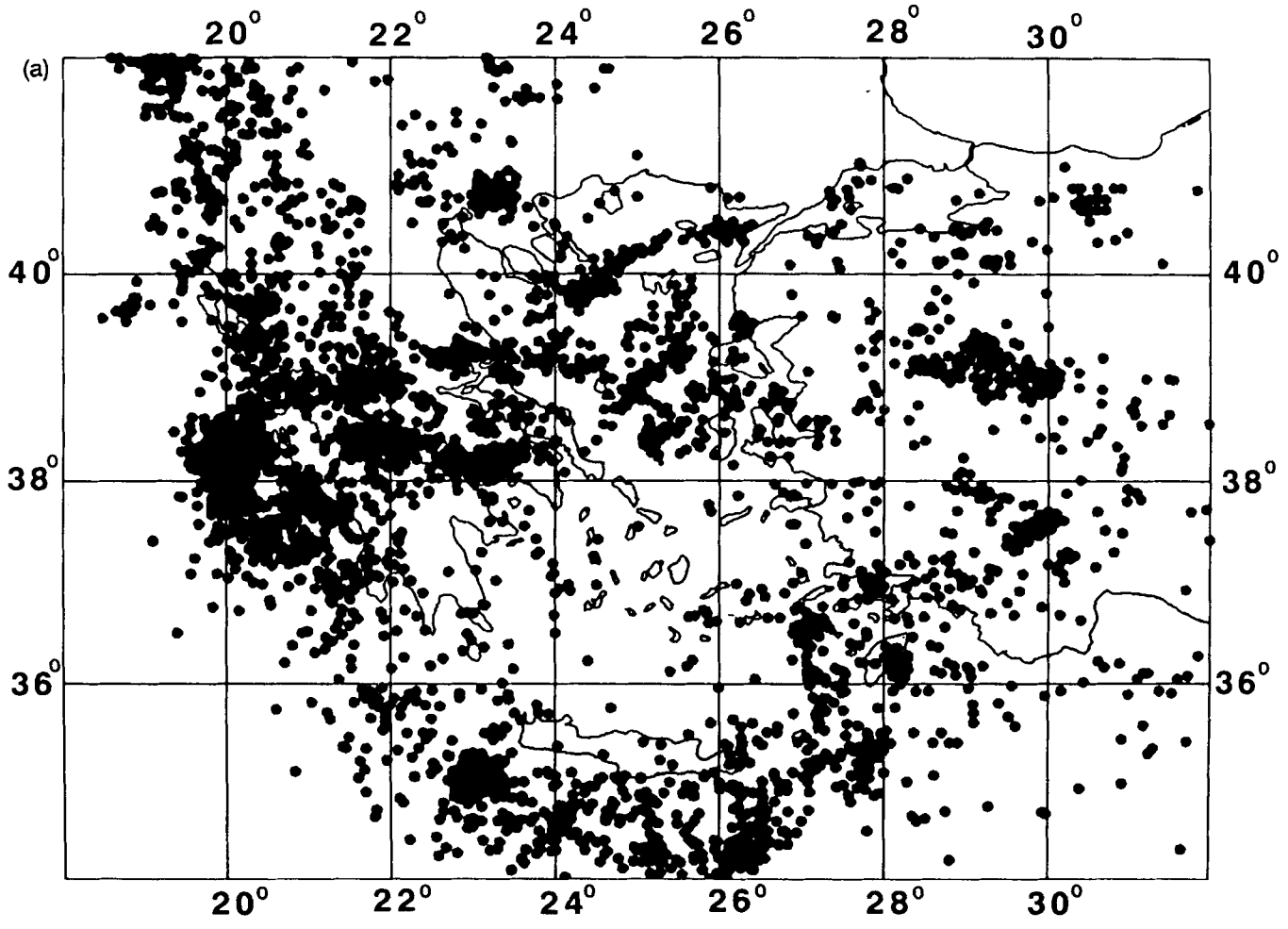

Figure 1(a). Positions of all epicentres of earthquakes with depths between 0 and 50 km reported by the USGS PDE during the period 1963 to 1988 (after Taymaz *et al.* 1991a).

attenuation using Futterman's (1962) operator, with $t^* = 1$ s for P and $t^* = 4$ s for SH. As explained by Fredrich *et al.* (1988), uncertainties in t^* mainly affect source duration and seismic moment, rather than source orientation or centroid depth. Seismograms were weighted according to the azimuthal distribution of stations, such that stations clustered together were given smaller weights than those of isolated stations (McCaffrey & Abers 1988). The inversion routine then adjusts the strike, dip, rake, centroid depth and source-time function, which is described by a series of overlapping isosceles triangles (Nábělek 1984) whose number and duration I selected. My experience with the inversion routine was very similar to that of Nelson *et al.* (1987), Friedrich *et al.* (1988) and Molnar & Lyon-Cáen (1989). I found that estimates of the strike, dip, rake and centroid depth were relatively independent of each other. Thus if one parameter was fixed at a value within a few degrees or km of its value yielded by the minimum misfit of observed and synthetic seismograms, the inversion routine usually returned values for the other parameters that were close to those of the minimum misfit solution. Uncertainty in the average velocity structure above the source leads directly to an uncertainty in centroid depth, which I estimate to be about ±2 km for the range of depths involved in this study. The velocity structure I used is given in Table 2. The estimate of seismic moment clearly depended on the duration of the source-time function, and to some extent on centroid depth and velocity structure. As my main interest is in source orientation and depth, I did not concern myself much with uncertainties in seismic moment, which in most cases is probably about 30 per cent. I estimated the lengths of the time functions by increasing the number of isosceles triangles until the amplitudes of the later ones became insignificant. The seismogram lengths I selected for inversion were sufficient to include the reflected phases pP, sP and sS. I examined the P waves for PcP arrivals, where they were anticipated within the selected window, but this phase was never of significant amplitude.

3 UNCERTAINTIES IN SOURCE PARAMETERS

Having found a set of acceptable source parameters, I followed the procedure described by McCaffrey & Nábělek (1987), Nelson *et al.* (1987), Fredrich *et al.* (1988), Molnar & Lyon-Cáen (1989), Taymaz (1990), Taymaz *et al.* (1990), Taymaz *et al.* (1991a), Taymaz, Eyidoğan & Jackson (1991b) and Taymaz & Price (1992), in which the inversion routine is

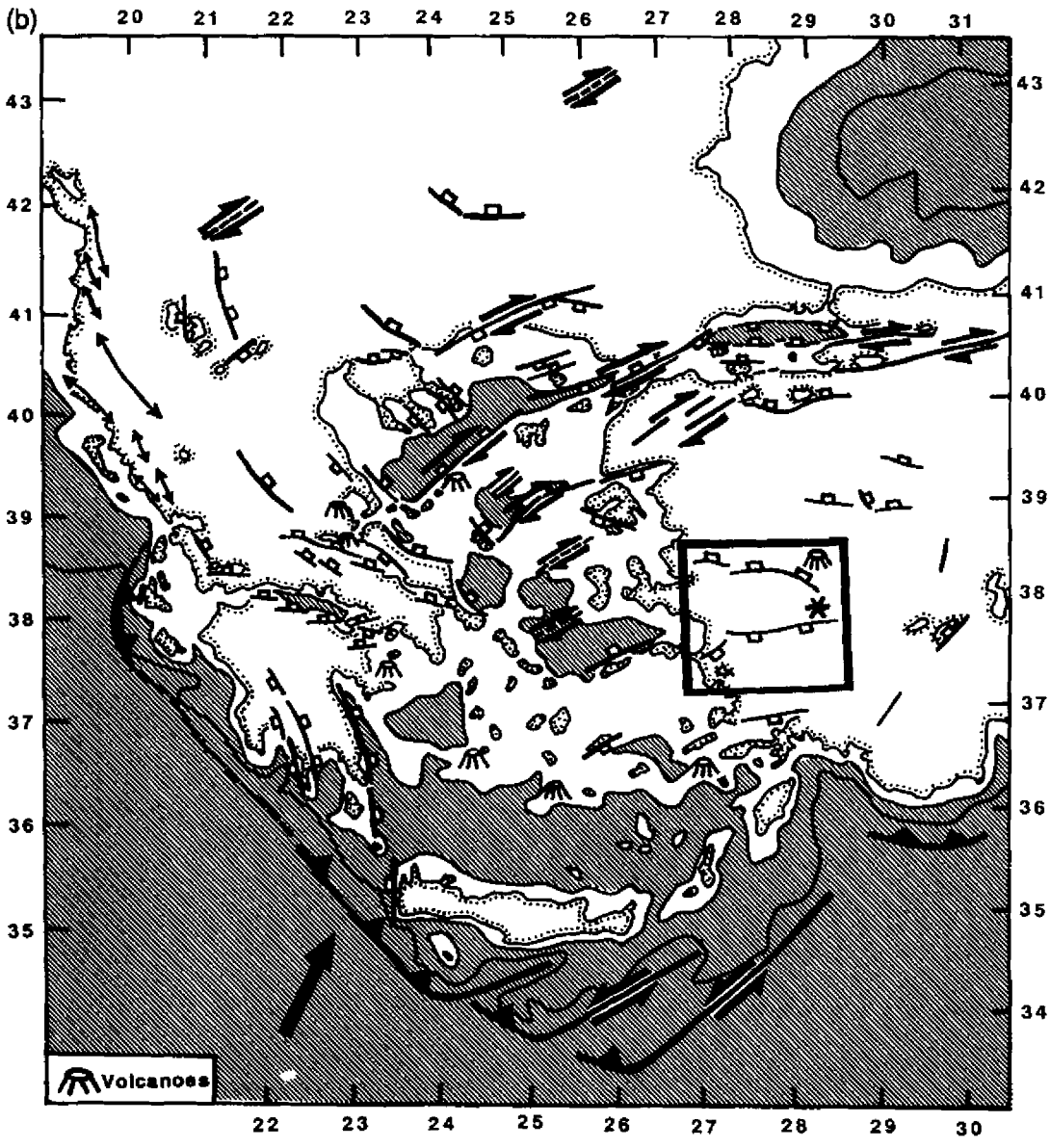

Figure 1(b). Summary sketch of the faulting and bathymetry in the Aegean region, compiled from observations of Taymaz *et al.* (1991a), Lybéris (1984), Le Pichon *et al.* (1984), Şaroğlu, Emre & Boray (1987) and Mercier *et al.* (1989). Normal faults are shown with open blocks on the downthrown side: many of these in the central Aegean have large strike–slip components, which are shown by heavy black arrows. Most of the normal faults are not as continuous as they are shown here, but are typically segmented on a scale of 15–20 km (see Roberts & Jackson 1991). This map shows only faults that are large, and are clearly associated with major topographic and bathymetric features or with earthquakes. Many smaller faults, including several in central Greece that are antithetic to the major graben-controlling fault systems, and some in western Turkey that have an approximately N–S strike (see Şengör, Görür & Şaroğlu 1985) have been omitted. Strike–slip faults that are shown as dashed lines have been identified on the basis of focal mechanisms alone. Double-headed arrows in NW Greece and Albania are the axes of major anticlines visible on satellite images. The Hellenic Trench is marked as a thrust with filled triangles on the hanging wall. The large black arrow in the SW is the direction of convergence in the Hellenic Trench near SW Crete (from Taymaz *et al.* 1990). Bathymetric contours are at 500 and 200 m, and shaded below 500 m. The area outlined by a solid line shows the region featured in the present work. Epicentre of Çubukdağ earthquake of 1986 October 11 is marked by an asterisk.

used to carry out experiments to test how well individual source parameters are resolved. I investigated one parameter at a time by fixing it at a series of values either side of its value yielded by the minimum misfit solution, and allowing the other parameters to be found by the inversion routine. I then visually examined the quality of fit between observed and synthetic seismograms to see whether it had deteriorated from the minimum misfit solution. In this way I was able to estimate the uncertainty in strike, dip, rake and depth for each event. In common with the authors cited

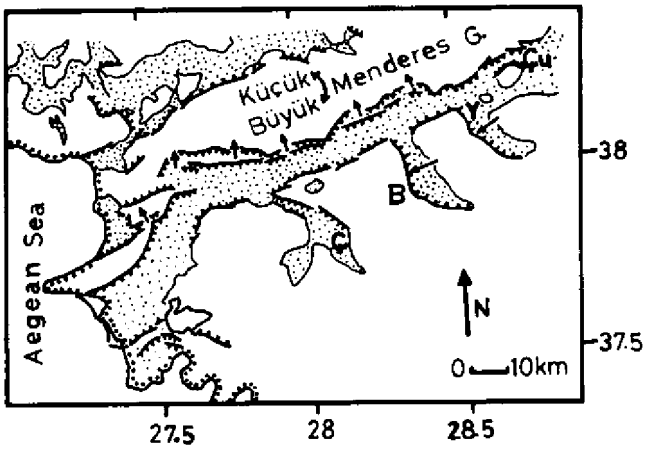

Figure 1(c). Normal faults and Neogene basins (stippled) around the Büyük Menderes graben (modified after Roberts 1988). Letters correspond to towns mentioned in the text: Ç: Çine, B: Bozdoğan, Y: Yenice, Çu: Çubukdağ. Arrows in the Neogene basins show the direction of regional bedding dip.

above, I believe this procedure gives a more realistic quantification of likely errors than the formal errors derived from the covariance matrix of the solution.

4 OUTLINE OF GEOLOGY—THE BÜYÜK MENDERES GRABEN

The Çubukdağ earthquake occurred in the vicinity of the Büyük Menderes graben (Fig. 1b–d). The main east–west trending part of the Büyük Menderes graben extends a total distance of about 125 km (Fig. 1c). Along most of its length, the north side of the graben is bounded by two approximately parallel normal fault systems. The southernmost of the two fault systems bounds the present valley floor, and runs along the base of the topographic escarpment on the North side of the Büyük Menderes valley; the second bounds the uplifted and tilted Neogene basin (also known as the North Büyük Menderes Basin) which is trapped between the two fault systems (Fig. 1c). Three main valleys (Yenice, Bozdoğan and Çine basins) drain the South side of the Büyük Menderes graben. Two of the cross-graben, the Yenice and Bozdoğan valleys are bounded on their West sides by large east-dipping normal faults trending approximately N–S. The direction of tilting observed in the Neogene sediments, the development of alluvial fans (now inactive)

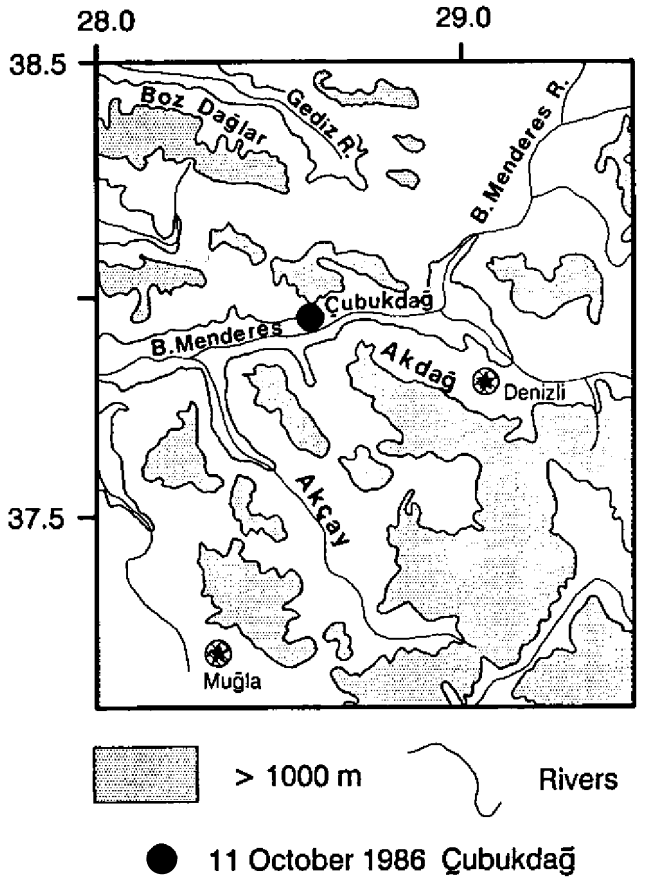

Figure 1(d). Topography of the Çubukdağ region. The Büyük Menderes graben, the main valleys and drainage patterns have a marked topographic expression. Stars mark the locations of the main cities.

on the west side of the graben, and the morphology of the range fronts (in the field and on Landsat images) suggests that the main graben bounding faults, which have also been active in recent times, are along the west side of the graben. The Çine basin was also fault bounded, but only along part of its north–east margin (see Roberts 1988 and Fig. 1c). The normal faults around the Büyük Menderes graben are discontinuous along strike, and were broken up into approximately linear fault segments which range in length from 2 to 30 km. The fault segments are linked in one of two ways: either by intersecting at angles to each other, or by overlapping in 'en'-echelon arrays. Fault segmentation was shown to have important implications for drainage and

Figure 2(a). Minimum misfit solutions for the Çubukdağ earthquake of 1986 October 11. This figure shows the radiation patterns and synthetic waveforms for the minimum misfit solution returned by the inversion procedure, as well as the observed waveforms. For the purposes of display, waveform amplitudes have been normalized to that of an instrument with a gain of 3000 at a distance of 40°. Solid lines are observed waveforms, and the inversion window is identified by vertical bars. Synthetic waveforms are dashed lines. The station code is identified to the left of each waveform, together with an upper case letter, which identifies its position on the focal sphere, and a lower case letter that indicates the type of instrument (w = WWSSN long period; d = GDSN long period). The vertical bar beneath the focal sphere shows the scale in microns, with the lower case letter indicating the instrument type, as before. The source time function is shown in the middle of the figure, and beneath it is the time scale used for the waveforms. Focal spheres are shown with *P* and *SH* nodal planes, in lower hemisphere projection. Station positions are indicated by letter, and are arranged alphabetically clockwise, starting from north. *P* and *T* axes are marked by solid and open circles, respectively. Beneath the header at the top of the figure, which shows the date, geographical location and surface wave magnitude, are five numbers which show the strike, dip, rake, centroid depth and seismic moment (in units of 10^{16} Nm) of the minimum misfit solution.

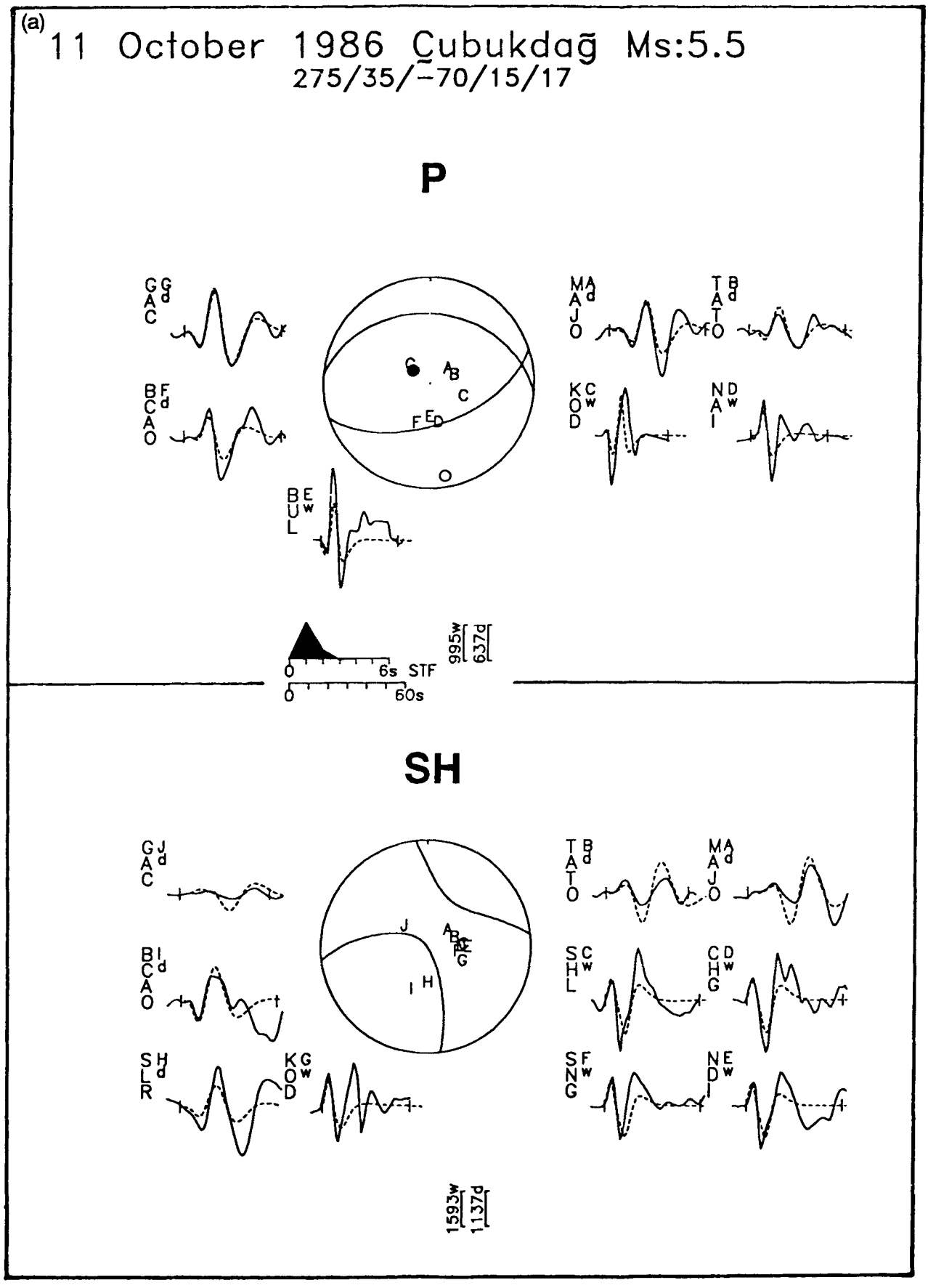

sediment distribution along the footwalls of active graben, and behind the footwalls of inactive and eroding graben. Multiple generations of slickensides were also associated with several of the fault plane exposures around the graben (Roberts 1988). He reported that the majority of the observed fault plane dips were in the range of 43°–60°, with an average value for all of the fault planes of about 49°.

Most of the hot springs in the Büyük Menderes graben

Most of the hot springs in the Büyük Menderes graben are associated with the surface trace of the main graben bounding faults. Oxburgh, O'Nions & Hill (1986) studied the He^{+3} isotope content of the hot springs associated with large normal faults in Western Turkey and central Greece. Their work showed that at least some of the hot springs have mantle helium signatures, suggesting a connection between the upper mantle and the surface, which in the upper crust is most likely to be along the large normal faults. In the Büyük Menderes graben, hot springs are sometimes associated with areas where fault segments overlap, or where two fault segments with different strikes intersect. Although all of the hot springs observed in the Büyük Menderes valley are along the North side of the graben, there is also evidence of a large hot spring on the South side of the graben (Şimşek 1984; Roberts 1988).

5 EARTHQUAKE SOURCE MECHANISM

The minimum misfit solution for this earthquake is shown in Fig. 2(a). The nodal planes of this solution are compatible with all first motion *P* polarities, with a compressional onset at north (IST) and nodal onsets at southern stations suggesting a relatively steep dip to a nodal plane dipping south (Fig. 2b). The minimum misfit solution indicates dominant normal faulting with small strike–slip component. The *P* and *SH* pulses are simple at all azimuths and characteristic of normal faulting with a shallow focal depth. There is good coverage of the focal sphere at all azimuths, for both first motion and waveform data. However, I was unable to achieve a satisfactory match of amplitudes of later arrivals for both *P* and *SH* waves at some azimuths, and I believe they are due to propagation path effects rather than source complexities.

Fig. 2(c) summarizes some of the tests that I have carried out to compare various parameters. The first row of Fig. 2(c) contains 3*P* and 3*SH* seismograms from Fig. 2(a), and shows the minimum misfit solution returned by the inversion routine. In row 2, I fixed the strike, dip and rake to that of Dziewonski *et al.*'s (1987) solution, and inverted for depth, moment and source-time function. The best double-couple mechanism found by the centroid–moment tensor inversion of Dziewonski *et al.* (1987) differs from my solution by 45° in strike, 22° in dip and 31° in rake for the northern-dipping nodal plane. However, for the southern-dipping nodal plane the only significant difference is in our rake which is not very well constrained by the Harvard CMT solution (see Table 1). These differences are outside the estimated errors in my solution, and their solution violates some of the first motion readings (Fig. 2b), and produces a worse fit to the waveforms, particularly wrong polarities for the *SH* waveforms at TATO, CHG and GAC whose position on the focal sphere is quite close to one of the nodal surfaces.

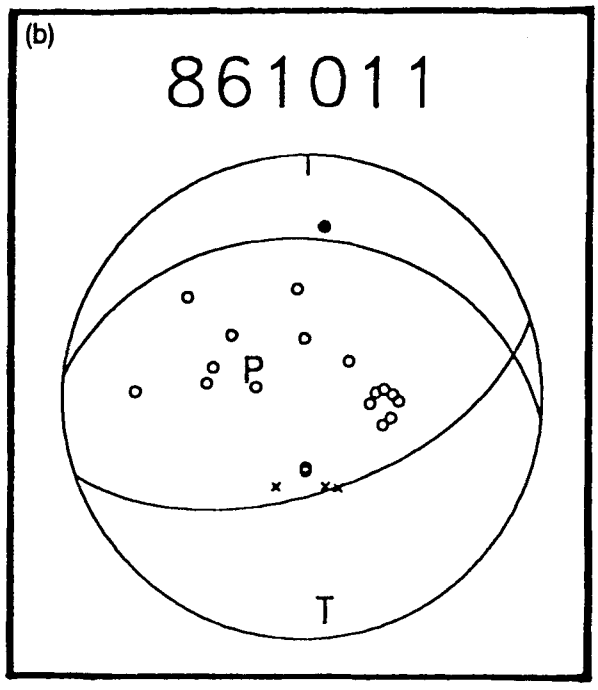

Figure 2(b). Lower hemisphere equal area projections of first-motion polarity data. Station positions on the focal sphere have been plotted using the same velocity below the source (6.8 km s^{-1}) that was used in our waveform inversion procedure. Filled circles are compressional first motions, open are dilatational, and nodal readings are marked with *x*. Nodal planes are those of the minimum misfit solutions. Above the sphere is the date of the event (year, month, day). Below the sphere are both the nodal planes which show the strike, dip and rake of the minimum misfit solution.

Dziewonski *et al.*'s (1987) seismic moment value ($M_O = 36 \times 10^{16}$ Nm) is more than twice that obtained in this study ($M_O = 17 \times 10^{16}$ Nm). Rows 3 and 4 display waveforms from inversion in which all source parameters were free to change except the centroid depth, which was fixed to values of 20 and 25 km. Note that the values of strike, dip and rake are little different in rows 3–4 from those in row 1, however, deeper focal depths produce a worse fit to waveforms due to delayed seismic phases. In general, the observed fit between the observed and synthetic waveforms is clearly worse in rows 2–4 than in row 1.

I carried out many experiments of the sort illustrated in Fig. 2(c), and based on these, I estimate the source parameters and uncertainties of the 1986 October 11 Çubukdağ earthquake to be: strike 71° ± 5°; dip 57° ± 5°; rake −103° ± 15° and depth 15 ± 3 km (although this does not include uncertainty related to velocity structure).

6 DISCUSSION AND CONCLUSIONS

The strike of the south-dipping nodal plane of the minimum misfit solution is close to the local trend of the graben.

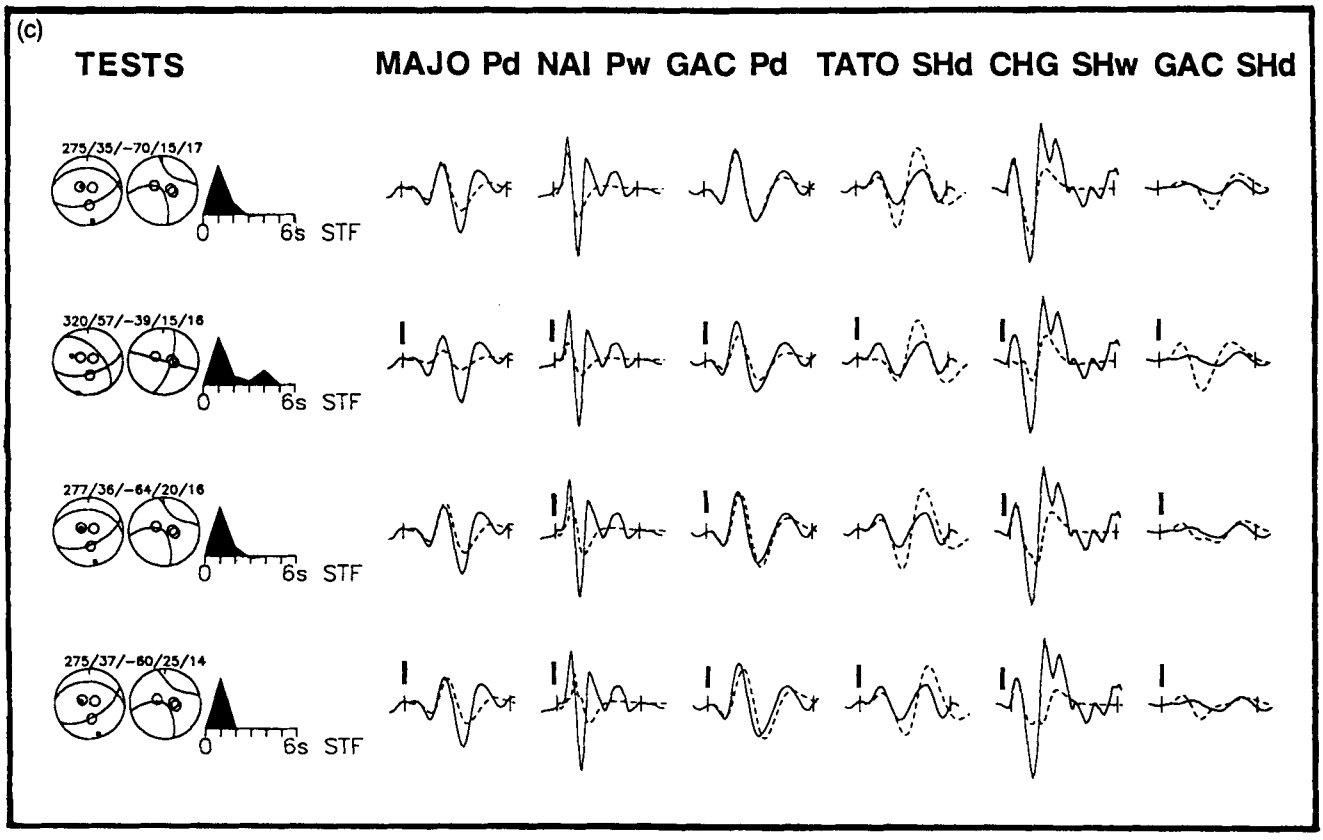

Figure 2(c). In this figure each row shows a selection of waveforms from a run of the inversion program. The stations are identified at the top of each column, with the type of waveform marked by *P* or *SH* and followed by the instrument type. At the start of each row are the *P* and *SH* focal spheres for the focal parameters represented by the five numbers (strike, dip, rake, depth and moment), showing the positions on the focal spheres of the stations chosen. The displayed waveforms are in the same convention as above, but in this type of figure the large bars show matches of observed to synthetic waveforms that are worse than in the minimum misfit solution. The top row shows waveforms from the minimum misfit solution. In second row the strike, dip and rake were fixed to the values of Dziewonski *et al.* (1987), while the other parameters were left free. In rows 3–4 the depth has been held fixed at values of 20 and 25 km respectively, while the other parameters were left free.

Roberts (1988) shows that the major bounding fault lies to the north of the graben, therefore I have taken the south-dipping nodal plane as the fault plane. He reports that the dip of the surface fault exposures is in the range 43°–60°. The dip of the south-dipping nodal plane of the Çubukdağ event is 57°, in agreement with these observations (Fig. 1b–c and Table 1). Furthermore, Roberts (1988) concluded that the oldest sediments in the area around the Büyük Menderes graben are probably about 13–10 Ma, and outcrop in the Samos and Kuşadası–Söke basins and the Bozdoğan, Yenice, Çine and Büyük Menderes graben.

Table 1. Source parameters of the Çubukdağ earthquake of 1986 October 11.

Origin Time (h m s)	Location Lat. N(°)	Long. E(°)	m_b	M_s	Nodal Plane 1 Strike (°)	Dip (°)	Rake (°)	Nodal Plane 2 Strike (°)	Dip (°)	Rake (°)	Centr. Depth (km)	M_o $\times 10^{16}$ (Nm)	
09:00:10.9	37.94	28.56	5.4	5.5	275	35	−70	71	57	−103	15	17	a
					320	57	−39	74	58	−140	15	36	b

a. This study.
b. After Dziewonski *et al.*(1987).

Table 2. Source velocity structure used.

Date (d m y)	V_p (kms^{-1})	V_s (kms^{-1})	Density (kgm^{-3})	Thickness (km)
11.10.1986	6.00	3.45	2780	10
	6.80	3.92	2910	half-space

ACKNOWLEDGMENTS

I would like to thank Andrew Smith for many helpful discussions and improvements to an early version of this paper, and Steven Roberts for a copy of his PhD. I am grateful to R. McCaffrey and G. Abers for allowing me to use their waveform inversion program. I am also grateful to the National Earthquake Information Centre and the US Geological Survey for making GDSN data available on CD-ROM. This work was supported by the Turkish Ministry of Higher Education, Taymaz family and Department of Earth Sciences, Cambridge University. Cambridge Earth Sciences contribution no. 2067.

REFERENCES

Barka, A. A. & Kadinsky-Cade, C., 1988. Strike-slip fault geometry in Turkey and its influence on earthquake activity, *Tectonics*, **7**, 663–684.

Brooks, M. & Ferentinos, G., 1980. Structure and evolution of the Sporadhes basin of the north Aegean trough, Northern Aegean Sea, *Tectonophysics,* **101,** 25–54.

Dewey, J. F., Hempton, M.R., Kidd, W. S. F., Şaroğlu, F. & Şengör, A. M. C., 1986. Shortening of continental lithosphere: the neotectonics of Eastern Anatolia: a young collision zone, in *Collision Tectonics,* pp. 3–36, Eds Coward, M.P. & Ries, A. C., Spec. Publ. Geol. Soc. Lond., vol. 19, Blackwell Scientific Publications, Oxford.

Dziewonski, A. M., Ekström, G., Woodhouse, J. H. & Zwart, G., 1987. Centroid-moment tensor solutions for October–December 1986, *Phys. Earth planet. Interiors,* **48,** 5–17.

Fredrich, J., McCaffrey, R. & Denham, D., 1988. Source parameters of seven large Australian earthquakes determined by body waveform inversion, *Geophys. J.,* **95,** 1–13.

Futterman, W. I., 1962. Dispersive body waves, *J. geophys. Res.,* **67,** 5279–5291.

Lalechos, N. & Savoyat, E., 1979. La sédimentation Néogéne dans le Fossé Nord Egéen, *6th colloquium on the Geology of the Aegean region,* vol. 2, pp. 591–603.

Le Pichon, X., Lybéris, N. & Alvarez, F., 1984. Subsidence history of the North Aegean trough in *Geological Evolution of the Eastern Mediterranean,* pp. 727–741, eds Dixon, J. E. & Robertson, A. H. F., Spec. Publ. Geol. Soc. Lond., vol. 17, Blackwell Scientific Publications Oxford.

Lybéris, N., 1984. Tectonic evolution of the North Aegean trough, in *Geological evolution of the Eastern Mediterranean,* pp. 709–725, Eds Dixon, J. E. & Robertson, A. H. F., Spec. Publ. Geol. Soc. Lond., vol. 17, Blackwell Scientific Publications, Oxford.

McCaffrey, R. & Abers, G., 1988. SYN3: A program for inversion of teleseismic body wave forms on microcomputers, *Air Force Geophysics Laboratory Technical Report,* AFGL-TR-88-0099, Hanscomb Air Force Base, MA.

McCaffrey, R. & Nábělek, J. 1987. Earthquakes, gravity, and the origin of the Bali Basin: an example of a nascent continental fold-and-thrust belt, *J. geophys. Res.,* **92,** 441–460.

McKenzie, D., 1978. Active tectonics of the Alpine–Himalayan belt: the Aegean Sea and surrounding regions, *Geophys. J. R. astr. Soc.,* **55,** 217–254.

Mercier, J. L., Sorel, D., Vergely, P. & Simeakis, K., 1989. Extensional tectonic regimes in the Aegean basins during the Cenozoic, *Basin Res.,* **2,** 49–71.

Molnar, P. & Lyon-Cáen, H., 1989. Fault plane solutions of earthquakes and active tectonics of the Tibetan Plateau and its margins, *Geophys. J. Int.,* **99,** 123–153.

Nábělek, J. L., 1984. Determination of earthquake source parameters from inversion of body waves, *PhD Thesis,* M.I.T., Cambridge, Massachusetts.

Nelson, M. R., McCaffrey, R. & Molnar, P., 1987. Source pararameters for 11 earthquakes in the Tien Shan, Central Asia, determined by *P* and *SH* waveform inversion, *J. geophys. Res.,* **92,** 12 629–12 648.

Oxburgh, E. R., O'Nions, R. K. & Hill, R. T., 1986, Helium isotopes in sedimentary basins, *Nature,* **324,** 632–635.

Philip, H., Cisternas, A., Gvishiani, A. & Gorshkov, A., 1989. The Caucasus: an actual example of the initial stages of continental collision, *Tectonophysics,* **161,** 1–21.

Roberts, S., 1988. Active Normal Faulting in Central Greece and Western Turkey, *PhD Thesis,* University of Cambridge, UK.

Roberts, S. & Jackson, J., 1991. Active normal faulting in central Greece: an overview, in *The Geometry of Normal Faults,* 125–142, Eds Roberts, A. M., Yielding, G. & Freeman, B., Spec. Publ. Geol. Soc. Lond., vol. 56, Blackwell Scientific Publications, Oxford.

Şaroğlu, F., Emre, Ö. & Boray, A., 1987. *Türkiye Diri Fay Haritası,* MTA, Ankara, Turkey.

Şengör, A. M. C., Görür, N. & Şaroğlu, F., 1985. Strike slip faulting and related basin formation in zones of tectonic escape: Turkey as a case study, in *Strike slip deformation, basin formation, and sedimentation,* pp. 227–264, Society of Economic Paleontologists and Mineralogists, Tulsa, No. 37.

Şimşek, S., 1984. The Aydin–Germencik–Ömerbeyli geothermal field of Turkey, *Seminar on Utilization of geothermal energy for electric power production and space heating,* United Nations Economic Commission for Europe, Florence, Italy.

Taymaz, T., 1990. Earthquake Source Parameters in the Eastern Mediterranean Region, *PhD Thesis,* University of Cambridge, UK.

Taymaz, T., Jackson, J. A. & Westaway, R., 1990. Earthquake mechanisms in the Hellenic Trench near Crete, *Geophys. J. Int.,* **102,** 695–731.

Taymaz, T., Jackson, J. A. & McKenzie, D., 1991a. Active tectonics of the north and cenral Aegean Sea, *Geophys. J. Int.,* **106,** 433–490.

Taymaz, T., Eyidoğan, H. & Jackson, J. A., 1991b. Source parameters of large earthquakes in the East Anatolian Fault Zone (Turkey), *Geophys. J. Int.,* **106,** 537–550.

Taymaz, T. & Price, S., 1992. The 1971 May 12 Burdur earthquake sequence, SW Turkey: a synthesis of seismological and geological observations, *Geophys. J. Int.,* **108,** 589–603.